Recent Res. Devel. Biomed. Eng., 1 (2002) : 15-31 ISBN: 81-7895-013-8

Multiresolution signal decomposition and its applications to electrogastric signals

Hualou Liang[1] and Zhiyue Lin[2]
[1]Center for Complex Systems & Brain Sciences, Florida Atlantic University, Boca Raton, FL 33431
[2]University of Kansas Medical Center, Department of Medicine, Kansas City, Kansas 66160

Abstract

In recent years there has been a considerable development in the use of multiresolution signal decomposition methods in biomedical signal processing. These methods analyze signals at different scales or resolution and thus are well suited for non-stationary signal analysis. In this paper, we first provide a description of two multiresolution methods, i.e., wavelet transform and Empirical Mode Decomposition (EMD) employed so far for electrogastric signal processing. We then illustrate two of their applications in detail to show the power of these methods. we finally conclude considering some future developments.

Correspondence/Reprint request: Dr. Zhiyue Lin, University of Kansas Medical Center, Dept of medicine – 4035D, 3901 Rainbow Boulevard, Kansas City, KS 66160-7350. Tel: 913-588-4025, Fax: 913-588-3975, E-mail: zlin@kumc.edu

2 Introduction

In the human stomach, there exists electrical activity that regulates the contractions of the stomach. Gastric myoelectric activity consists of slow waves and spikes. The gastric slow wave originates in the corpus and propagates distally towards the pylorus. The gastric slow wave is omnipresent and its frequency in humans is about 3 cycles per minute (cpm). The frequency and propagation of gastric contractions are determined by the gastric slow wave. Spikes, bursts of rapid changes in gastric myoelectric activity, are directly associated with antral contractions. The antral muscles contract when slow waves are superimposed with spike potentials. Abnormality in slow wave rhythmicity is called gastric dysrhythmia which includes bradygastria (regular frequency below 2 cpm), tachygastria (regular frequency above 4 cpm), and arrhythmia (irregular rhythmicity). It is the time variation of the frequency that may provide useful information in the assessment of patients with motility disorders.

Gastric myoelectric activity can be measured serosally and/or cutaneously. Serosal electrodes can record both slow waves and spikes. It, however, is invasive and thus has limited applications. The cutaneous recording is obtained by placing electrodes on the abdominal skin over the stomach. It is usually called electrogastrogram (EGG) [1]. The EGG is very attractive due to its noninvasiveness. It has been shown [2, 3, 4] that the cutaneous electrodes are able to pick up the rhythm of the gastric slow wave, and that the dominant frequency of the EGG represents the frequency of the gastric slow wave. The EGG therefore provides reliable information about gastric myoelectric activity.

Compared with other electrophysiological measurements such as electrocardiogram (ECG), the EGG has a low signal-to-noise ratio. The EGG is usually contaminated by respiratory, motion, and cardiac signals and possible myoelectric activity from other organs. As a result, direct visual interpretation of the EGG time series is almost impossible. Advanced signal processing methods are needed for studying the gastric electrical behavior. The multiresolution signal decomposition methods analyze signals at different scales or resolution and thus are ideally suited for analyzing the non-stationary signal such as electrogastric signal.

The rapidly evolving field of multiresolution signal decomposition methods [5, 6, 7, 8, 9] has witnessed several excellent contributions to the electrogastric signal analysis. Sun et al [10, 11] described the Continuous Wavelet Transform (CWT) for the analysis of electrogastric signals and the detection of spike. It was observed amplitude changes in the slow wave during spike activity and a detection accuracy of up 96% from the cutaneous EGG recordings based on the scored serosal spike activities simultaneously recorded. Similarly, Wang et al [12] proposed a Wavelet Packets method for the identification of gastric dysrhythmias. It was found that this approach provides higher frequency resolution than the short-time Fourier transform and Wigner-Ville distribution methods. Recently, we developed two multiresolution signal decomposition methods for electrogastric signal analysis. One is based on the wavelet transform in conjunction with the fuzzy set theory for the cancellation of stimulus artifact in the serosal recordings of the gastric myoelectric activity during gastric electrical stimulation. Another called Empirical Mode Decomposition [9] method which appears to be uniquely suitable for nonlinear, non-stationary data analysis. Experimental results show this method, combined with instantaneous frequency analysis, can be used effectively to separate, identify and remove contamination from a wide variety of artifactual sources in EGG recordings.

This chapter provides an overview of the applications of the multiresolution signal decomposition methods to the study of the electrogastric signal, with emphasis on our own recent work. The structure of this review is the following: in Section 2 we provide the necessary theoretical background on multiresolution signal decomposition; then in Section 3, we illustrate the applications of multiresolution signal decomposition to electrogastric signals. Finally, in Section 4, we conclude considering some future developments.

3 A description of multiresolution signal decomposition

Multiresolution representations are very effective for analyzing the information content of signals. It is computed by decomposing the original signal using a wavelet orthonormal basis, and can be interpreted as a decomposition using a set of independent frequency channels having a spatial orientation tuning. A wavelet representation lies between the spatial and Fourier domains. There is no redundant information because of the orthogonality of the wavelet functions. The detailed mathematical development of the algorithm used in this presentation has been presented by Mallat [5].

3.1 Wavelet transform

The wavelet transform has emerged as an exciting new tool for statistical signal processing. The wavelet domain provides a natural setting for many applications involving biomedical signals, such as ECG analysis [13,14], edge detection of medical image [15], classification [16], and chronobiological signal [17]. In contrast to the Short Time Fourier Transform (STFT) with fixed window size, the WT has a varying window size, being wide for low frequencies and narrow for the high ones, thus leading to an optimal time-frequency resolution in all the frequency ranges [18]. Moreover, owing to the fact that windows are adapted to the transients of each scale, wavelets do not need stationarity. The attractive properties of the wavelet transform have led to powerful signal processing methods based on simple scalar transformations of individual wavelet coefficients.

The CWT of a one-dimensional signal $x(t) \in L^2(R)$ with respect to a mother wavelet $\phi(t)$ is defined as [19,18]

$$W_x(a,b) = \frac{1}{\sqrt{|a|}} \int_{-\infty}^{+\infty} x(t)\psi(\frac{t-b}{a})dt \tag{1}$$

where a, b (a, $b \in \mathcal{R}$ and $a \neq 0$) are the scale and translation parameters, respectively. The CWT $W_x(a, b)$ gives a time-scale decomposition (where the scale can be considered as similar in functionality to frequency) of the signal $x(t)$ with a indexing the scale and b indexing time in the original signal space. Dilated versions of $\phi_{a,b}(t)$ will match low frequency components and on the other hand, contracted versions will match high frequency oscillations. Hence, the CWT exhibits the property of "zooming" in on the sharp temporal variations in a signal.

The main disadvantages of the CWT are redundancy and computational complexity. In practice, the wavelet transform scale and translation parameters are discretized and for fast numerical implementation the scale normally varies along a dyadic sequence

$(2^s)_{s \in Z}$. This yields the *Dyadic Wavelet Transform* [6]:

$$W_x(s,n) = \frac{1}{\sqrt{2^s}} \int_{-\infty}^{+\infty} x(t)\psi(\frac{t-n}{2^s})dt \tag{2}$$

For a wavelet centered at time zero and frequency f_0, the wavelet coefficient $W_x(s,n)$ characterizes the signal $x(t)$ around the time n and frequency $2^{-s} f_0$. An example of the wavelet transform of a typical serosal recording of the electrogastric signal during gastric pacing is illustrated in Fig. 1. When the scale decreases, the wavelet transform has a rapid decay to zero in the regions where the signal is regular. Clearly, the irregular structures occupied by the stimulus artifacts and the gastric signals can be accurately localized from the time-scale distribution of the recording.

Singularities and irregular structures often carry the most important information contained in a signal. The WT can focus on localized signal structures with a zooming procedure that progressively reduces the scale parameter. A remarkable property of the WT is that it is able to characterize the singularity of a function at a point [6]. The local maxima of the wavelet transform modulus maxima provide enough information to detect and analyze all singularities. It has been shown that the wavelet transform, W_x (s, n) is proportional to the first derivative of the lowpass filtered version of signal $x(t)$ [7]. As a consequence, for any given scale s, the modulus maxima and modulus minima of the wavelet transform $W_x(s, n)$ correspond respectively to the points of sharp variation and slow variation of the smoothed signal at scale s. Thus, the local shape of irregular structures in the signal can be characterized by the evolution of wavelet local maxima across scales. This multiscale characterization of the signal was called by Mallat et al. [6, 7] the Wavelet Transform Modulus Maxima (WTMM) representation. Fig. 2 demonstrates such a multiscale decomposition of the signal shown in Fig.1 (top panel). Fig. 2(top) shows its wavelet transform computed on seven scales, whereas the Fig. 2(bottom) shows the corresponding modulus maxima of the wavelet transform. The WTMM representation of a signal records the values and locations of local maxima of its

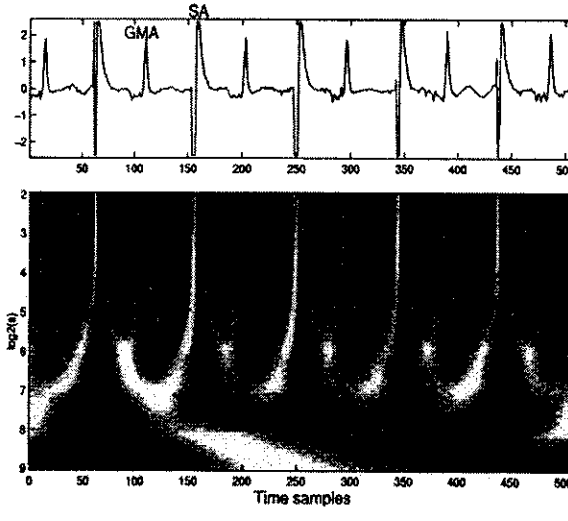

Figure 1. The wavelet transform shows the time-scale distribution (bottom panel) of a serosal recording (top plot). The scale axis is logarithmic. Black, grey and white points correspond respectively to positive, zero and negative wavelet coefficients. Note the localisation of the stimulus artifacts and the gastric signals. SA: stimulus artifact and the gastric signals. SA: stimulus artifact; GMA: gastric myoelectric activity.

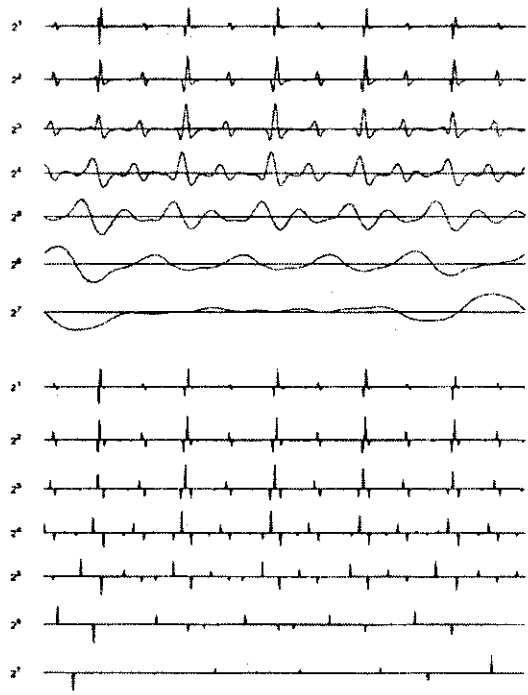

Figure 2. (top) Wavelet transform of the signal shown in Fig. 1 (top) computed at seven scales,with the quadratic spline wavelet shown in Fig.3(a). (bottom) Wavelet transform modulus maxima. At each scale, each Dirac indicates the position of a modulus maximum and the value of the wavelet transform at the corresponding location.

wavelet transform modulus. In [7], it is showed that a signal could be reconstructed, with good approximation, from the WTMM. For details of the description of the WTMM representation and the efficient implementation of the reconstruction algorithm, reader can refer to the original work [6, 7].

In our applications described in the following section, the realization of the wavelet transform follows with that of Mallat's approach [6, 7]. The mother wavelet we used is a quadratic spline wavelet (Fig. 3 (a)) due to its similarity with the stimulus artifact. It is the first derivative of the cubic spline function shown in Fig. 3 (b). In fact, there are many different functions suitable as wavelets, each having different characteristics that are more or less appropriate depending on the application. Irrespective of the mathematical properties of the wavelet to choose, a basic requirement is that it looks similar to the patterns we want to localize in the signal. This allows a good localization of the structures of interest in the wavelet domain.

Notice that Wavelet bases are one particular family of bases that represent piecewise smooth signals effectively. Other bases can be constructed to approximate different types of signals such as highly oscillatory waveforms. Wavelet Packets [20] and Local Cosine Bases [21] are two examples. The wavelet basis decomposes the frequency axis in dyadic intervals whose sizes have an exponential growth, as shown by Fig. 4b. The wavelet packet basis as a generalization of the fixed dyadic construction decomposes the frequency axis in separate intervals whose bandwidths are of various sizes, as shown in Figure 4c. If the signal properties change over time, it is preferable to isolate different time intervals with translated windows. Local cosine bases are constructed by multiplying these windows with

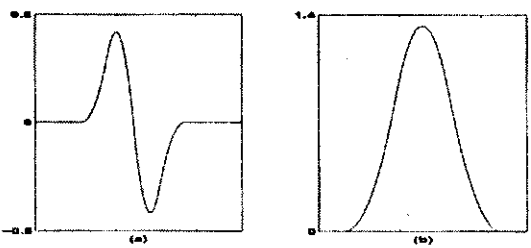

Figure 3. Quadratic spline wavelet function with compact support and one vanishing moment. It is the first derivative of the cubic spline function in (b).

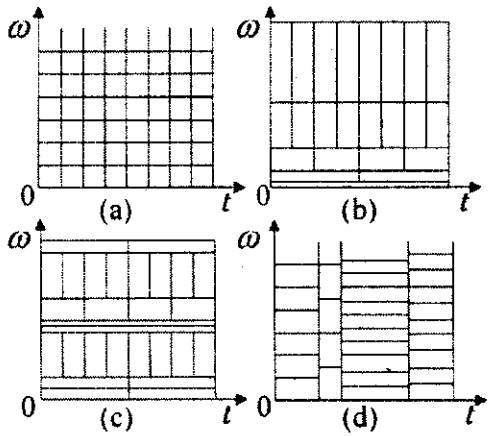

Figure 4. The time-frequency tiling of (a) the STFT, (b) the WT, (c) the wavelet packet basis, and (d) the local cosine basis. The tiling of the STFT and the WT is fixed, whereas the tiling of the wavelet packet and local cosine basis may be adapted to suit a particular application.

cosine functions. Local cosine and wavelet packets bases are dual families of bases. Local cosine bases segment the time axis and are uniformly translated in frequency whereas wavelet packets divide the frequency axis and are uniformly translated in time.

The fundamental difference between the aforementioned multiresolution signal decomposition methods is in the manner in which they partition the time-frequency plane. The STFT has a fixed tiling; once specified, each cell has an identical aspect ratio. The tiling of the WT is variable - the aspect ratio of the cells varies such that the frequency resolution is proportional to the center frequency. This tiling has been shown to be more appropriate for many signals, but the partition is nonetheless still fixed. Both the wavelet packets and local cosine bases provide the adaptive tilings - an over-complete set of tilings are provided as alternatives, and the best for a given application is selected. An illustration of the time-frequency tiling subtended by the STFT, the WT, the wavelet packets and local cosine bases is shown in Figure 4.

3.2 Empirical mode decomposition

The EMD method was initially proposed in the study of fluid mechanics [22], and found immediate applications in biomedical engineering [23]. The central idea of this method is the sifting process to decompose any given signal into its fundamental modes, those basic building blocks that make up complicated data. If we were to apply a Fourier decomposition to the signal, then the basis functions are linear combinations of sine and cosine waves, which would be the case if the signal were linear. Fourier analysis therefore merely works well for strictly linear, stationary random functions of time. With the EMD approach, the basis functions themselves are nonlinear functions which can be extracted directly from the data. In other words, an adaptive basis called Intrinsic Mode Function (IMF) can be found. This technique, combined with the Hilbert transform, has been successfully applied for artifact reduction in EGG recordings [9].

The decomposition is developed from the simple assumption that any data consist of different simple intrinsic modes of oscillations. A signal to be an IMF must satisfy two criteria: (a) in the whole data set, the number of local maxima and the number of local minima must either equal or differ by at most one; (b) at any point, the mean of its upper and lower envelopes equals zero.

Given these two definitive requirements of an IMF, the problem of interest is how we derive an IMF from a given data $X(t)$, e.g. EGG recording, as shown in Fig. 5(a) in thin solid line. The solution essentially consists of three major steps:

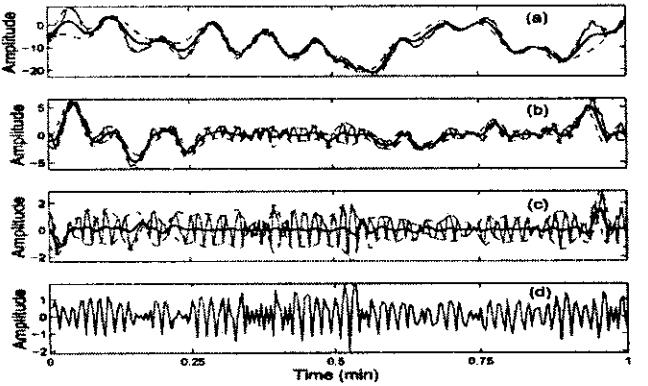

Figure 5. Illustration of the sifting process: (a) the original data in thin solid line, with the upper and lower envelopes in dotted lines and the mean plotted in thick solid line; (b) the difference $X_1(t)$, the envelopes of maxima and minima and their mean; (c) results shown after two iterations; (d) the final IMF is shown.

step 1: we construct two smooth splines connecting all the maxima and minima of $X(t)$ to get its upper envelope, $X_{up}(t)$, and its lower envelope, $X_{low}(t)$, which are plotted with dotted lines in Fig. 5(a); The extrema can be simply found by differentiation of the data sampled at discrete points and then determine where the sign flips. Once the extrema are identiifed, all the maxima are connected by cubic spline line as the upper envelope. Repeat the procedure for the local minima to produce the lower envelope. The upper and lower envelopes should cover all the data between them.

step 2: we subtract the mean of these two envelopes from the data to get their difference $X_1(t)$,

$$X_1(t) = X(t) - (X_{up} + X_{low})/2; \tag{3}$$

In Fig. 5(a) we plot the mean of envelopes in thick solid line.

step 3: we repeat steps (1) and (2) for $X_1(t)$ until the resulting signal meets the criteria of an intrinsic mode.

These three steps give the general scenario of the sifting process. We can see that the signal $X_1(t)$, as shown in Fig. 5(b) with thin solid line, is not an IMF, for there are a few negative local maxima and positive minima. This situation is improved by two more interactions, as shown in Fig. 5(c), the mean is still not zero. Keep iterating, the convergent signal denoted as $C_1(t)$, Fig. 5(d), is the first IMF of data $X(t)$, which has a zero local mean.

We then treat the residue $R_1(t) = X(t) - C_1(t)$ as new data that are subject to the sifting process as described above, yielding the second IMF from $R_1(t)$. The procedure continues until finally a mode becomes less than a predetermined small number or the residue becomes non-oscillatory. The original signal $X(t)$ can thus be expressed as follows:

$$X(t) = \sum_{j=1}^{N} C_j(t) + R_N(t), \tag{4}$$

where N is the number of IMFs, $R_N(t)$ is the final residue which can be either the mean trend or a constant, and functions $C_j(t)$ are nearly orthogonal to each other, and all have

zero means. By the nature of the decomposition procedure, the technique decomposes data into N fundamental components, each with distinct time scale. More specifically, the first component has the smallest time scale which corresponds to the fastest time variation of data. As the decomposition process proceeds, the time scale increases, and hence, the mean frequency of the mode decreases. Since the decomposition is based on the local characteristic time scale of the data to yield adaptive basis, it is applicable to nonlinear and non-stationary data in general and in particular, EGG data considered in the following section.

Once all the IMFs' are found, the instantaneous frequency of each component can be readily obtained by utilizing the Hilbert transform, which can be used later for signal identification. A more detailed explanation of the Hilbert transform is presented in Appendix A.

4 Applications of multiresolution representation to electrogastric signals

4.1 Stimulus artifact cancellation in the serosal recordings of gastric myoelectric activity

Previous studies [24, 25] have shown that electrical stimulation of the stomach (i.e. gastric pacing) with appropriate parameters is a promising method for treatment of gastroparetic patients. The recording of gastric myoelectric activity by serosal electrodes is often used to evaluate the effect of stimulation. However, the major problem with the measurement of gastric myoelectric activity during gastric pacing is the stimulus artifacts which are often superimposed on the serosal recording and make analysis difficult [26]. Here We describe a wavelet transform-based method for the reduction of stimulus artifacts in the serosal recordings of gastric myoelectric activity. The key of this method lies in the use of the fuzzy set theory to select the stimulus artifact-related modulus maxima in the wavelet domain.

The serosally recorded gastric myoelectric signal during gastric pacing mainly consists of gastric slow waves, stimulus artifacts and a considerable amount of noise due to muscular and respiratory activities, etc. The key to cancel the stimulus artifacts from gastric myoelectric recordings using WT is how to select the desired wavelet transform coefficients for reconstruction of gastric slow waves. This is the choice of which coefficients to keep and which to eliminate. Our solution lies in the use of the fuzzy set theory and associated operators [27] to extract gastric slow waves related maxima in wavelet domain, which has been shown its efficacy for the edge detection of medical image [15] and the extraction of fetal electrocardiogram (ECG) [14].

As stated, the stimulus artifacts contained in the serosal recordings result from an external pulse generator. The stimulus artifacts may differ from the stimuli in magnitudes and locations, but the information about locations of the stimuli is steadily available. Such *a priori* information can be best exploited with the fuzzy set theory to accommodate the spatial ambiguity (the uncertainty of location) of stimulus artifacts. The spatial ambiguity, arising mostly from the time delay of propagation, is the main motivation to take advantage of fuzzy membership functions.

Specifically, the modulus maxima locations, with some ambiguity, are compared at each scale between the stimuli and the gastric myoelectric recording during pacing. A

triangular fuzzy membership function, μ (s, n), centered on the maxima location n at scale s, is employed to represent the ambiguity. The fuzzy intersection between two fuzzy sets, μ_p (s, n) and μ_g (s, n) of the stimuli and the gastric myoelectric recording during pacing respectively, corresponds to the locations of the modulus maxima of stimulus artifacts, which can be expressed as

$$M_{pg}(s,n) = \begin{cases} \mu_p(s,n) \cap \mu_g(s,n), & n \in \mathcal{D} \\ 0 & \text{elsewhere} \end{cases} \tag{5}$$

The $M_{pg}(s, n)$ consists of the membership values in the interval [0, 1]. $\mathcal{D}$ denotes a set of local maxima. Its complementary set, $M_{\bar{p}g}(s,n)$ indexing to the locations of the modulus maxima of the gastric myoelectric activity (GMA), is therefore written as

$$M_{\bar{p}g}(s,n) = \begin{cases} 1 - M_{pg}(s,n), & n \in \mathcal{D} \\ 0 & \text{elsewhere} \end{cases} \tag{6}$$

The fuzzy decision is finally made to form the desired modulus maxima of the GMA, as follows:

$$W_g^m(s,n) = W_x^m(s,n) \times M_{\bar{p}g}(s,n) \tag{7}$$

where $W_x^m(s,n)$ denotes the modulus maxima of the wavelet transform $W_x(s,n)$. Fig. 6 illustrates the above fuzzy decision making procedure. The essence of the fuzzy-based technique is to determine the fuzzy intersection between the stimulus and the stimulus artifact contained in the gastric myoelectric recording in their WTMM representations so that it provides tolerance with respect to their misalignments in the modulus maxima.

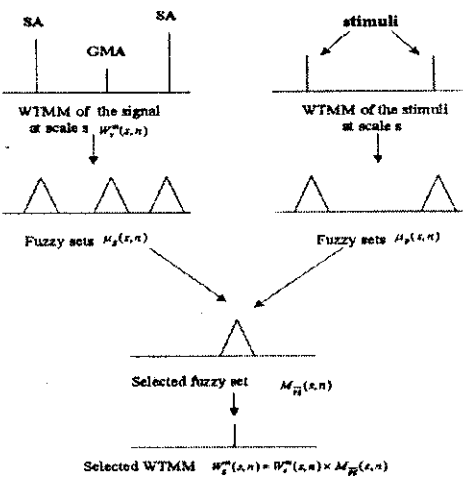

Figure 6. Fuzzy decision making schema for estimation of the modulus maxima of gastric myoelectric signal. SA: stimulus artifact; GMA: gastric myoelectric activity.

Let us remark a critical point when implementing the fuzzy-based algorithm. This is the choice of triangular fuzzy membership function. The width of the membership function at the lowest scale was empirically set to be 2 samples on each side of the modulus maxima, which gave us best results. Once the fuzziness width at the lowest scale is determined, it must be proportionally varied by a factor of two with the scale to ensure more uncertainty at the higher scales. The choice of the proportional factor of two is due to the use of dyadic wavelet transform, which can be

easily understood from Fig. 7 where the evolution of a single point x_0 across scales falls with the *cone of influence*. The *cone of influence* of x_0 for any scale s is defined by $|x - x_0| \leq K_s$ [6], where K is the support of the mother wavelet. Its definition clerly reveals that the neighborhood of x_0 proportionally varies whith the scale.

From the above analysis, we design a four-stage procedure for the stimulus artifact cancellation as follows.

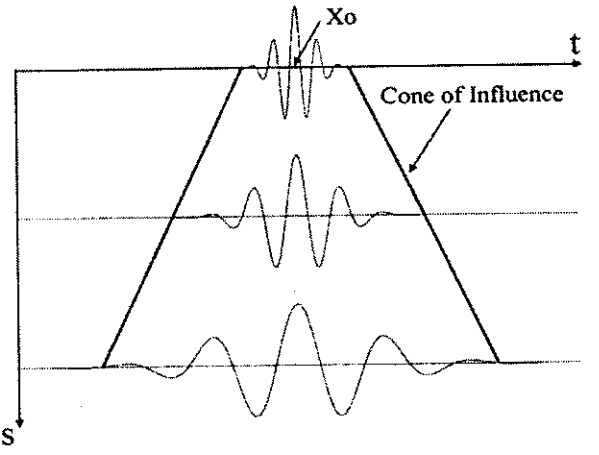

Figure 7. The cone of influence of x_0 in the time- scale plane.

1) *Analysis stage*: WTMM representations of the serosal recordings and of the stimuli in the time-scale plane are obtained using WT.

2) *Denoising stage*: For the WTMM representation of the serosal recordings, the local maxima with amplitudes below certain threshold for each scale are removed, where the threshold is adaptive determined with the scale-dependent threshold estimation procedure called SureShrink [28]. It was showed in [6] that the WTMM curves of the noise decay across scales at least at a rate of $1/2^s$ or even do not propagate to larger scales. Consequently, in application of denoising, we can remove noise of a signal by removing all the WTMM of which the amplitude decreases when the scale increases. This step is expected to remove noise and thus reduce spurious spikes contained in the signal which could be otherwise mistaken as stimulus artifacts.

3) *Estimation stage*: the modulus maxima of the gastric myoelectric signal are estimated using a fuzzy-based technique, as detailed above.

4) *Reconstruction stage*: the gastric myoelectric signal is reconstructed from the estimated modulus maxima [7].

The procedure we described so far is for one-channel stimulus artifact cancellation. Application to multichannel recordings is straightforward by applying the above procedure for each channel recorded since the stimulus artifacts contained in all the channels are generated by the same pacemaker. Once the modulus maxima of stimulus artifacts are extracted, such information can be repeatedly used to cancel stimulus artifacts by other channels where available.

Results from both single- and multichannel serosally recorded myoelectric signals during gastric pacing are presented to demonstrate the efficiency of the above proposed method for the cancellation of stimulus artifacts. Three typical serosal recordings with different energy levels of the stimulus artifact during gastric pacing are presented in Fig. 8(a)-(c). The reconstructed gastric signals are depicted in Fig. 8(d)-(f). We can see from Fig. 8 that the most dominant characteristics of gastric signals are well preserved after the cancellation of stimulus artifacts.

One example of applications to the multichannel recordings is presented in Fig. 9. In Fig. 9 (a), we show 3-channel recordings during gastric pacing, with corresponding

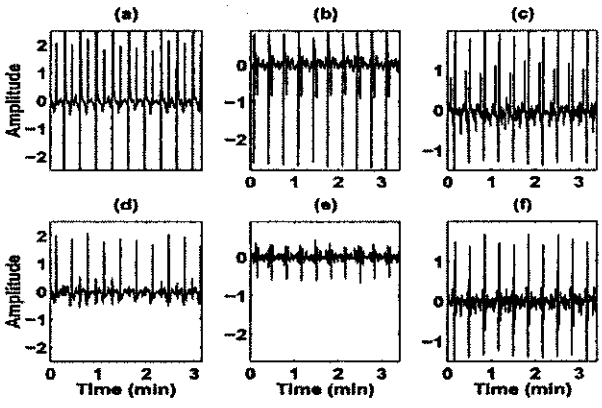

Figure 8. Three typical results of cancellations of stimulus artifacts. (a)-(c) The serosal recordings during gastric pacing. (d)-(f) the reconstructed gastric myoelectric signals.

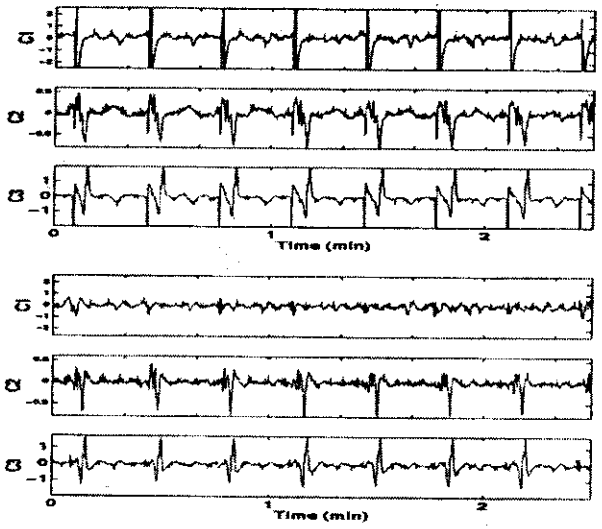

Figure 9. Cancellation of stimulus artifacts in the multichannel recordings. Top: 3-channel recordings. Bottom: the reconstructed gastric myoelectric signals.

extracted gastric signals in Fig. 9(b). It is clearly observed that the stimulus artifacts in the recordings are greatly reduced.

4.2 Artifact reduction of EGG [9]

As described in the Introduction, the EGG is a combination of the gastric signal and considerable noise. Severe contamination of gastric signal in the electrogastrogram (EGG) by respiratory, motion, cardiac signals, and possible myoelectric activity from other organs poses a major challenge for EGG interpretation and analysis. Here we present the experimental results of application of the EMD method for removing a variety of artifacts from EGG recordings with great success.

The artifact reduction procedure basically consists of three steps. **The first step** is to decompose the data into a number of IMF components by the empirical mode decomposition. **The second step** is to perform the Hilbert transform to each of the IMF components to obtain its instantaneous frequency. **The final step** is to identify the artifactual or relevant signals on the basis of prior knowledge, and then extract cleaner EGG. Two examples are described to illustrate the applications of EMD method to reduce artifact in the EGG recording and to extract slow wave from EGG [9].

In the first application, a 10-min EGG recording from a healthy subject, as shown in Fig. 10(a), was used in the experiment. Fig. 11 shows the resulting IMF components. The Hilbert transforms of these IMF components give their instantaneous frequencies shown in Fig. 12. The first three components correspond to heart beating, respiratory artifact and harmonic signal respectively. Component 4 should be the ongoing gastric

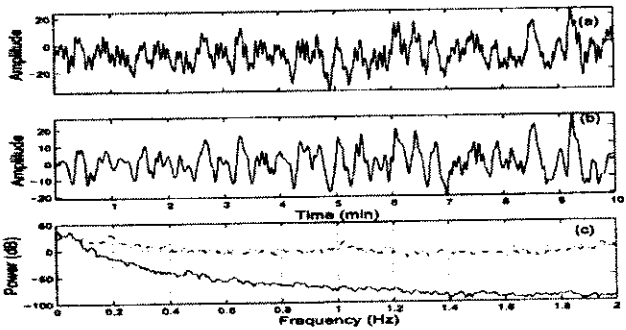

Figure 10. A typical EGG recording from one healthy subject before and after artifact reduction and their power spectra: (a) the original signal; (b) the extracted clean EGG; (c) the power spectra of signals in (a) (dot-dashed line) and (b) (solid line).

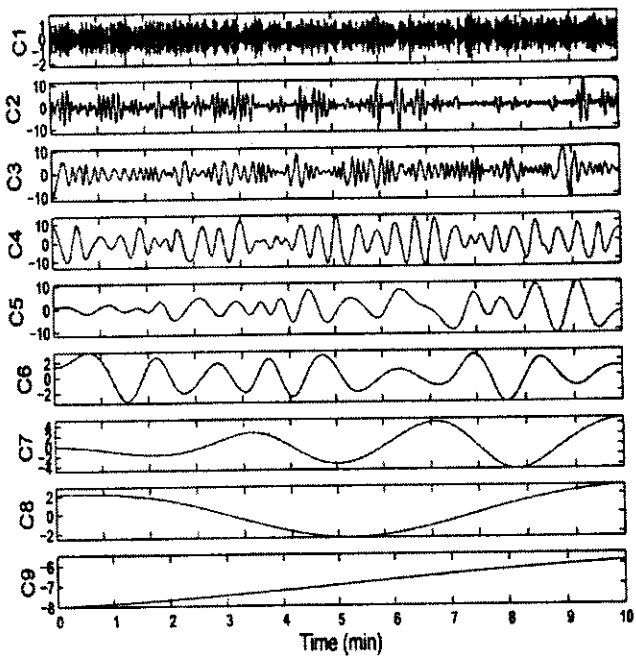

Figure 11. The IMF components from the EGG data in Fig. 10(a).

slow wave around 3 cpm which clearly reflects the non-stationary nature of gastric activity.

It is even more convinced by scrutinizing its frequency content of each component, as shown in Fig. 13. The peak frequencies of component 1, 2, 3 and 4 are successively 1.02 Hz, 0.2 Hz, 0.1 Hz and 0.05 Hz, which correspond to heart beating, respiratory artifact, harmonic signal and gastric slow wave, respectively. For comparison, we plot the extracted gastric signal (Component 3 and 4) in Fig. 10(b). The frequency contents of the original EGG and extracted gastric signal are shown in Fig. 10(c). We can observe from these figures that the gastric signal component is effectively extracted whereas other noise and artifacts are greatly reduced.

In the second application, a 10-min EGG recording with heavy motion interference, which is a more difficult artifact to remove, was selected. In contrast to the aforesaid examples, we can see from the EGG recording as shown in Fig. 14(a), the weak gastric signal is mostly submerged in the motion artifacts, therefore, it is necessary to firstly use proper preprocessing method to weaken the power of motion interference, and then apply the EMD method. To tackle this thorny problem, we devised a preprocessing procedure by thresholding the raw EGG data $x(t)$ according to the following formula:

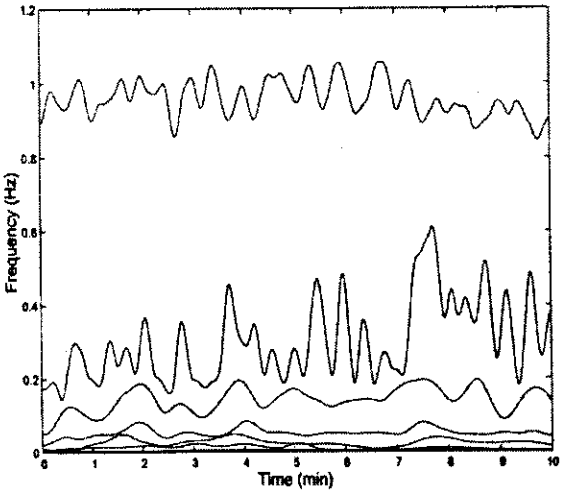

Figure 12. The instantaneous frequencies of the IMF components in Fig.11. There is considerable frequency variation, and indication that the EGG is not stationary.

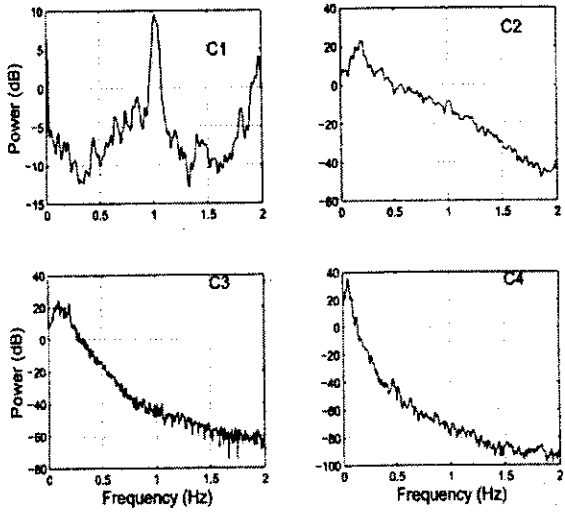

Figure 13. The power spectra of the first four IMF components, where the peak frequency in each subplot is 1.02 Hz, O.2 Hz, 0.1 Hz and 0.5 Hz respectively, which in turn correspond to heart beating, respiratory artifact, harmonic signal and gastric slow wave.

$$x(t) = \begin{cases} p1 & \text{if } x(t) > p1, \\ p2 & \text{if } x(t) < p2, \\ x(t) & \text{others} \end{cases}$$

where $p1$, $p2$, the applied thresholds as plotted in Fig. 14(a) in dashed lines, are respectively the mean $\pm$ 3 $\times$ (standard deviation) of the EGG segment without severe motion artifacts. By comparison of the power spectra of before (in thin solid line) and after (in dotted lines)thresholding the EGG data, as shown in Fig. 14(c), the power of EGG data is not or less affected. More sophisticated preprocessing method, of course, can be done by applying the adaptive thresholding approach [28]. However, we found this method is adequate for our purpose.

Following the empirical mode decomposition and signal identification procedure as stated above, the IMF components of the preprocessed EGG is presented in Fig. 15. The extracted gastric signal (component 4) is shown in Fig. 14(b), and its power spectrum is plotted in Fig. 14(c) in thick solid line. It is clearly observed that the motion artifacts and high frequency components in the EGG recording are greatly reduced.

5 Discussion and conclusion

In this chapter we have reviewed the recent developments and applications of the multiresolution signal decomposition methods to the analysis of electrogastric signals, with emphasis on the wavelet transform and empirical mode decomposition.

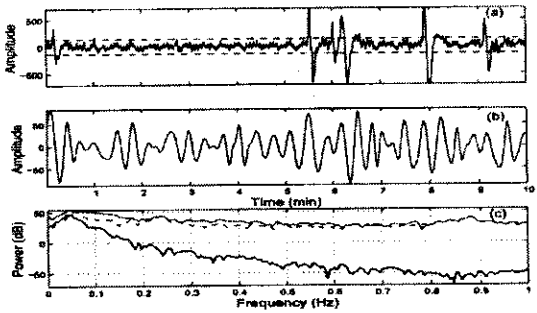

Figure 14. An EGG recording with motion artifacts before and after artifact reduction and their power spectra: (a) the original EGG recording, two dashed lines are the applied thresholds, discarding the values exceeding these limits; (b) the extracted clean EGG after removing the first two IMFs and the DC component; (c) the power spectrum of clean EGG (in thick solid line) in comparison with those of the original EGG data (in thin solid line) and preprocessed one (in dashed line), where the difference between the latter two is almost indiscernble implies that the gastric signal embedded in the EGG is not or less affected by our preprocessing procedure.

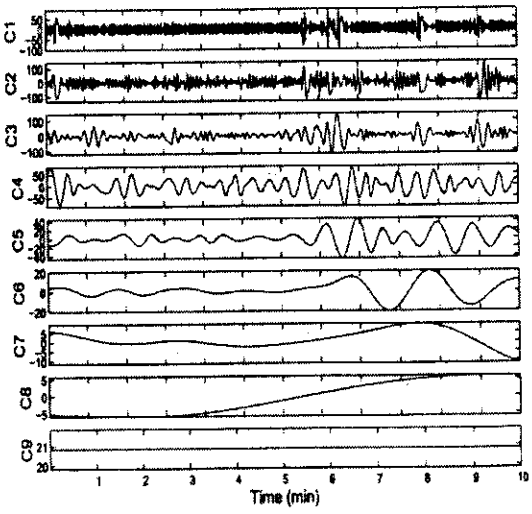

Figure 15. The nine IMF components obtained by the EMD method

We show that the wavelet transform can be effectively used for the cancellation of stimulus artifact in the serosal recordings of the gastric myoelectric activity during gastric electrical stimulation. The key of this method lies in the use of the fuzzy set theory to select the stimulus artifact-related modulus maxima in the wavelet domain. Two practical aspects of this method deserve further remarks. First, if the stimulus artifacts coincided with the gastric slow waves, the algorithm would not work well. However, it is not likely in most cases that both of their singularities are completely overlapped both in scale and in time. Second, if there are spikes in the serosal recording of gastric myoelectric activity, their modulus maxima similar to those of the stimulus artifact will also propagate to higher scales, which will be mistaken as stimulus artifacts. This problem needs further analysis.

The EMD method also exploits the extrema information to identify the intrinsic oscillatory modes, but the decomposition is directly based on the data. This method appears to be uniquely suitable for nonlinear, non-stationary data analysis since the decomposition is based on the local characteristic time scale of the data to yield the adaptive basis. The great advantage of the EMD is the effective use of the data, which is particularly useful where only limited data is available. Moreover, the decomposition components usually have more physically meaningful interpretation of the underlying dynamic processes. Yet, there are areas needing future attention. The cubic spline fitting adopted here has both overshoot and undershoot problems. The alternative is the higher-order spline program which

would be more time consuming and the improvement would probably be marginal. The end effects in both the spline fitting and the Hilbert transform need improvements, too. We further note that an additional step may have to be taken to preprocessing the EGG data before the use of EMD method when the the gastric signal embedded in stronger motion artifacts. This is because the EMD method is build on the identification of scale from successive of extrema [22]. If the gastric signals are phase locked with, and occur only at the maximum slope regions of the strong motion artifacts, then it will be difficult to recover the gastric signal. In this case, either a hard-threshold or differentiation of original data could be used before using the EMD method.

In summary, the multiresolution signal decomposition is a rapidly evolving field with great applications in many areas. The methods presented here have been proved to be useful for the study of electrogastric signals and should be also applicable to other biomedical signals.

6 Appendix A

The Hilbert transform has been widely used in order to obtain the analytic signal associated with the real signal $x(t)$, and, consequently, its instantaneous envelope and phase functions. The instantaneous frequency which is of interest in our present report can be further derived from the instantaneous phase, and its definition is given below [29].

Given a time series $x(t)$, the corresponding analytic signal is defined to be

$$z(t) = x(t) + iH[x(t)] = a(t)\exp[i\theta(t)], \tag{8}$$

where the $a(t)$ and $\theta(t)$ are the instantaneous amplitude and phase of the analytic signal $z(t)$, and the imaginary part $H[x(t)]$ is the Hilbert transform of $x(t)$:

$$H[x(t)] = \mathcal{P}[\frac{1}{\pi}\int_{-\infty}^{\infty}\frac{x(u)}{t-u}du].$$

Here, the notion $\mathcal{P}$ indicates the Cauchy principal value of the integral [29]. If $\mathcal{F}\{x(t)\}$ and $\mathcal{F}\{z(t)\}$ are respectively the Fourier transforms of $x(t)$ and $z(t)$, then the above relationship is expressed in the frequency domain by

$$\mathcal{F}\{z(t)\} = \begin{cases} 2\mathcal{F}\{x(t)\} & \text{if } \omega > 0, \\ \mathcal{F}\{x(t)\} & \text{if } \omega = 0, \\ 0 & \text{if } \omega < 0 \end{cases} \tag{9}$$

Thus, the analytic signal, which still retains the information content of its original real signal, can be obtained from Eq. 9. With the instantaneous phase, it is then possible to define in a unique way the concept of instantaneous frequency by

$$\omega(t) = d\theta(t)/dt \tag{10}$$

By virtue of the analytic signal, the given signal can be faithfully represented by the amplitude and the frequency as functions of time in a three-dimensional plot, in which

the amplitude ditribution on the time frequency plane is referred to as the Hilbert spectrum.

References

1. Alvarez, W.C., The electrogastrogram and what it shows, *J. Amer. Med. As-soc.*, 78, 1116-1118, 1922.
2. Smout, A.J.P.M., van der Schee, E.J. and J.L. Grashuis, What is measured in electrogastrography? *Dig. Dis. Sci.*, 25, 179-187, 1980.
3. Familoni, B.O., Bowes, K.L., Kingma, Y.J., et al., Can transcutaneous recordings detect gastric electrical abnormalities? *Gut*, 32, 141-146, 1991.
4. Chen, J., McCallum, R.W., Electrogastrogram: Measurement, Analysis and Prospective Applications, *Med. Biol. Eng. Comput.*, 29, 339-350, 1991.
5. Mallat S.G., A Theory for multiresolution signal decomposition - the wavelet representation, *IEEE Trans. Pattern Anal. Machine Intell.*, 11(7), 674-693, 1989.
6. Mallat S. and Hwang, W.L., Singularity detection and processing with wavelets, *IEEE Trans. Inform. Theory*, 32(2), 617-643, 1992.
7. Mallat S. and Zhong, S., Characterization of signals from multiscale edges, *IEEE Trans. Pattern Anal. Machine Intell.*, 14(7), 710-732, 1992.
8. Thakor N.V., Guo X.R., Sun Y.C., Hanley D.F., Multiresolution wavelet analysis of evoked-potentials, *IEEE Trans. Biomed. Eng.*, 40(11), 1085-1094, 1993.
9. Liang H., Lin Z., McCallum R.W., Artifact reduction in electrogastrogram based on empirical mode decomposition method, *Med. Biol. Eng. Comput.*, 38(1), 35-41, 2000.
10. Qiao W.W., Sun H.H., Chey W.Y., Lee K.Y., Continuous wavelet analysis as an aid in the representation and interpretation of electrogastrographic signals, *Annals of Biomed. Eng.*, 26(6), 1072-1081, 1998.
11. Akin A., Sun H.H., Time-frequency methods for detecting spike activity of stomach, *Med. Biol. Eng. Comput.*, 37(3), 381-390, 1999.
12. Wang Z.S., He Z.Y., Chen J.D.Z, Optimized overcomplete signal representation and its applications to time-frequency analysis of electrogastrogram, *Annals of Biomed. Eng.* , 26(5), 859-869, 1998.
13. Li C., Zheng C., and Tai C., Detection of ECG characteristic points using wavelet transform, *IEEE Trans. Biomed. Eng.*, 42(1), 21-28, 1995.
14. Khamene, A. and Negahdaripour S., A new method for the extraction of fetal ECG from the composite abdominal signal, *IEEE Trans. Biomed. Eng.*, 47(4), 507-516, 2000.
15. Setarehdan, S. K. and J. J. Soraghan, Automatic cardiac LV boundary detection and tracking using hybrid fuzzy temporal and fuzzy multiscale edge detection, *IEEE Trans. Biomed. Eng.*, 46(11), 1364-1378, 1999.
16. Bruce, L. M. and R. R. Adhami, Classifying mammographic mass shape using the wavelet transform modulus maxima method, *IEEE Trans. Biomed. Eng.*, 18(12), 1170-1177, 1999.
17. Chan, F. H. Y., B. M. Wu, F. K. lam, P.W..F.Poon, and A.M.S. Poon, Multiscale characterization of chrono-biological signals based on the discrete wavelet transform, *IEEE Trans. Biomed. Eng.*, 47(1), 88-95, 2000.
18. Chui, C., *An introduction to wavelets*. Academic press, San Diego, 1992.
19. Grossmann, A. and J. Morlet, Decomposition of hardy functions into square integrable wavelets of constant shape, *SIAM J. math.*, 15, 723-736, 1984.
20. Coifman, R.R., Y. Meyer, and M.V. Wickerhauser, Wavelet analysis and signal processing. In *Wavelets and their Applications*, pp. 153-178, Boston, 1992.
21. Malvar, H.S., The LOT: A link between block transform coding and multirate filter banks. In *Proc. IEEE Int. Symp. Circ. and Syst.*, pp. 835-838, Espoo, Finland, June 1988.
22. Huang, N.E., Shen, Z., Long, S.R., Wu, M.L.C., Shih, H.H., Zheng, Q.N., Yen, N.C., Tung, C.C. and Liu, H.H., The empirical mode decomposition and the Hilbert spectrum for

nonlinear and non-stationary time series analysis, *Proc. Roy. Soc. LOND A MAT*,454, 903-995, 1998.

23. Huang, W., Shen, Z., Huang, N.E. and Fung, Y.C., Engineering analysis of biological variables: An example of blood pressure over 1 day, *Proc. Nat. Acad. Sci. USA*, 95, 4816-4821, 1998.
24. Familoni, B.O., T.L. Abell, D. Nemoto, G. Voeller, A. Salem, O. Gabor, Electrical stimulation at a frequency higher than basal rate in human stomach, *Dig. Dis. Sci.*, 42, 885-891, 1997.
25. McCallum, R.W., J.D.Z. Chen, Z.Y. Lin, B.D. Schirmer, R.D. Williamms and R.A. Ross, Gastric pacing improves emptying and symptoms in patients with gastroparesis, *Gastroenterology*, 114, 456-461, 1998.
26. Lin, Z.Y., J.D.Z. Chen, and R.W. McCallum, Adaptive cancellation of stimulus artifacts in the gastric myoelectric recordings, in CD-ROM Proc. 18th IEEE Annual Conf. on EMBS, Amsterdam, The Netherlands, 1996.
27. Dubios, D. and H. Prade, *Fuzzy Sets and Systems: Theory and Applications*, New York: Academic and Harcourt Brace Jovanovich, 1980.
28. Donoho, D.L. and I.M. Johnstone, Adapting to unknown smoothness via wavelet shrinkage, *J. Am. Stat. Assoc.*, 90, 1200-1224, 1995.
29. Oppenheim, A. and Schafer, R., Digital Signal Processing. Prentice-Hall, New-Jersey, 1975.